Structural Variations within the Transferrin Binding Site on Transferrin-binding Protein B, TbpB*[S]

Charles Calmettes[‡], **Rong-hua Yu**[§], **Leslie P. Silva**[¶], **Dave Curran**[§], **David C. Schriemer**[¶], **Anthony B. Schryvers**[§¶1], **and Trevor F. Moraes**[‡2]

From the ‡Department of Biochemistry, University of Toronto, Toronto, Ontario M5S 1A8, Canada, the §Department of Microbiology & Infectious Diseases, University of Calgary, Calgary, Alberta T2N 4N1, Canada, and the ¶Department of Biochemistry & Molecular Biology, University of Calgary, Calgary, Alberta T2N 4N1, Canada

Pathogenic bacteria acquire the essential element iron through specialized uptake pathways that are necessary in the iron-limiting environments of the host. Members of the Gram-negative *Neisseriaceae* and *Pasteurellaceae* families have adapted to acquire iron from the host iron binding glycoprotein, transferrin (Tf), through a receptor complex comprised of trans-ferring-binding protein (Tbp) A and B. Because of the critical role they play in the host, these surface-exposed proteins are invariably present in clinical isolates and thus are considered prime vaccine targets. The specific interactions between TbpB and Tf are essential and ultimately might be exploited to create a broad-spectrum vaccine. In this study, we report the structure of TbpBs from two porcine pathogens, *Actinobacillus pleuro-pneumoniae* and *suis*. Paradoxically, despite a common Tf target, these swine related TbpBs show substantial sequence variation in their Tf-binding site. The TbpB structures, supported by docking simulations, surface plasmon resonance and hydrogen/deuterium exchange experiments with wild-type and mutant TbpBs, explain why there are structurally conserved elements within TbpB homologs despite major sequence variation that are required for binding Tf.

While colonizing or infecting the host, bacterial pathogens utilize surface proteins to acquire nutrients and interact with host components to survive the antibacterial properties of the host milieu. For bacteria, the acquisition of the essential nutrient iron is of critical importance as vertebrates sequester free iron within the extracellular milieu using specific iron carrying glycoproteins, lactoferrin (Lf), and transferrin (Tf)[3] (1).

To colonize, bacteria have selectively evolved with their host to express specific mechanisms for iron uptake. The pathogenic Gram-negative bacteria from the *Neisseriaceae* and *Pasteurel-laceae* families have developed a host Tf-specific iron uptake system mediated by a bacterial receptor complex, the Tf-binding proteins A and B (TbpA, TbpB) (2). TbpA is a TonB-dependent outer-membrane protein, strictly essential for iron uptake during bacteria infection (3). TbpA binds both of the holo or apo forms of Tf (4), and it is proposed to serve as a channel for iron transport across the outer membrane (5). TbpB, the second component of the receptor complex, is a surface exposed lipoprotein that binds holo-Tf in a selective manner (4, 6). This enables the bacterial receptor to recruit iron more efficiently from the partially iron-saturated forms of Tf *in vivo* (7). TbpB is essential for colonization of the host (8), and depending on the strain and species, TbpB-defective bacteria present several different growth-impaired phenotypes. TbpBs display species specificity (9), binding only to their host Tf, while the human Tf-receptor has no species specificity retrieving Tf through endocytosis where the low pH of the endosome drives the iron delivery from Tf (10, 11).

Surface lipoproteins such as TbpB have been targeted for vaccine development as they elicit a strong immune response, and antibodies to specific surface lipoproteins are bactericidal (12–14). Because TbpB functions to specifically associate with the host protein Tf, it is likely that the site of interaction may harbor a conserved binding interface (15) that could be exploited to create a broad spectrum vaccine.

Recently the structure of the TbpB from the porcine pathogen *Actinobacillus pleuropneumoniae* together with functional binding studies has illustrated that the residues from the site of interaction with porcine Tf (pTf) do not appear to be conserved among porcine pathogens (16). The structure illustrates that TbpB is a bilobed protein requiring the N-lobe domain for Tf binding function. Both the N- and C-lobe adopt a similar overall fold; the C-lobe is the most conserved domain in sequence along all TbpB proteins, while N-lobes show paradoxically a less well-conserved sequence even between strains targeting the same host and thus the same Tf (16).

A. pleuropneumoniae along with *Actinobacillus suis* and *Haemophilus parasuis* are important pathogens in pigs that share a common mechanism for acquiring iron directly from the host Tf (17–19). This parallels the situation with human pathogens in which *Neisseria meningitidis*, *Moraxella catarrhalis*, and *H. influenzae* acquire iron from human Tf through a conserved, highly specific interaction common to these species (15). In the absence of structural information for TbpBs from human pathogens, a study of TbpBs from porcine

---

pathogens provides the greatest opportunity to probe the details of this interaction and determine how a conserved interaction can be maintained in the face of considerable sequence diversity.

In this study, we describe crystal structures of two divergent TbpB receptors from the porcine pathogens *A. suis* (H57) and *A. pleuropneumoniae* (H87) and provide models of the pTf-TbpB complexes that are supported by hydrogen-deuterium exchange coupled to mass spectrometry (H/DX-MS) and binding experiments with site-directed mutant TbpBs.

EXPERIMENTAL PROCEDURES

Sequence Analysis of tbpB Genes—The *tbpB* genes from all of our clinical isolates of *A. pleuropneumoniae* and *A. suis* were amplified from whole colonies using a set of primers designed to bind ~100 bp outside of the gene. These sequences were combined with all of the unique publicly available *tbpB* sequences, and a ClustalW2 multiple sequence alignment was generated. The alignment was manually inspected and edited, and a bootstrapped neighbor-joining unrooted phylogenetic tree was generated from this alignment using the program Geneious.

Expression and Purification of Recombinant TbpB—Protein was expressed and purified essentially as described previously (16). The genes encoding TbpB from *A. suis* strain H57 (*As*H57) and *A. pleuropneumoniae* strain H87 (*Ap*H87) were cloned in to an expression vector encoding an N-terminal maltose-binding protein fusion partner containing a polyhistidine tag and a TEV cleavage site preceding the region encoding the mature TbpB protein. The recombinant fusion proteins were isolated on a pTf-Sepharose column as described previously (16) or by Ni-NTA chromatography. After cleavage by TEV protease the TbpB proteins were purified by Q-Sepharose chromatography as described previously (16).

Protein Crystallization—Purified *As*H57 and *Ap*H87 TbpBs were screened against the JSCG+ suite commercial screen using hanging drop vapor diffusion at 10 mg/ml. Initial *As*H57 TbpB crystals were observed in 0.2 M tri-potassium citrate pH 8.3 and 20% PEG 3350 then optimized with a 1:1 ratio sitting drop at 20 °C in a precipitant solution composed of 0.1 M Bis-Tris pH 5.5, 0.4 M lithium sulfate, 17% PEG 3350 and 20% glycerol yielding crystals in space group P2$_1$. *Ap*H87 TbpBs were first observed in 0.16 M calcium acetate, 0.08 M sodium cacodylate pH 6.5, 14.4% PEG 8000, and 20% glycerol and optimized at 20 °C using 0.16 M sodium acetate, 0.08 M calcium cacodylate pH 6.5, 23% PEG 3350 and 15% glycerol to yield crystals in space group C222$_1$. Unit cell dimensions and statistics are summarized in Table 1.

Structure Determination—Data were gathered on crystals frozen at 105 K on beamline 08ID-1 at the Canadian Light Source (CLS). Diffraction data sets of *As*H57 TbpB and *Ap*H87 TbpB were collected at a wavelength of 0.9795 Å using 1° oscillations with 360 and 300 images, respectively. Data were processed with XDS (20) to resolutions of 2.1 Å for *Ap*H87 TbpB and *As*H57 TbpB. The first structural model was obtained by molecular replacement based on *Ap*H49 TbpB (PDB code 3HOL) using PHASER (21), yielding an initial R_{work}/R_{free} 0.29/0.32 and 0.34/038 for *As*H57 and *Ap*H87, respectively. Final

models were generated following several rounds of model building and refinement using Coot (22) and Refmac5 (23) programs. A Ramachandran plot calculated 3.9% and 3.0% of residues in the allowed region and 0.4% and 0.2% as outliers, for *As*H57 and *Ap*H87 TbpB, respectively. The numbering of residues initiates with the first mature amino acid (Cys-1) remaining after signal peptide cleavage.

Surface Plasmon Resonance—Surface Plasmon resonance experiments were performed using BiacoreX (GE Healthcare) at 25 °C. Porcine transferrin was coupled to the sensor chip (CM5 research grade) via standard *N*-hydroxysuccinimde and *N*-ethyl-*N*-(dimethylaminopropyl) carbodiimide activation. Wild-type TbpB and mutant variants were diluted at various concentrations with the mobile phase buffer (10 mM Hepes pH 7.5, 150 mM NaCl, and 0.005% surfactant P20). Samples were injected as analytes at a flow rate of 20 μl/min, and bound analytes were subsequently removed by washing with the mobile phase at 90 or 240 s after the injection. Regeneration buffer (10 mM Hepes, pH 7.5, 2 M NaCl) was injected prior to each analyte injection. Kinetic constants were calculated from the sensorgrams using the simulated BiacoreX evaluation software, version 4.0.1 (Biacore). The AsH57, *Ap*H87, and *Ap*H49 TbpBs data were fitted to a "heterogeneous ligand" binding model. The *Ap*H87 TbpB R179E mutant was analyzed using the saturation method and fitted with a quadratic equation with BiacoreX evaluation software.

Docking Simulation—As the structure of TbpB bound to pTf has not yet been elucidated, the interaction was modeled using RosettaDock (24) incorporating the information generated by SPR analysis. RosettaDock was run in full atom mode, allowing spin around the axis connecting the two proteins, and using standard Monte Carlo movements. A custom program was written to allow experimentally determined important residues to be taken into account during a docking run. The general algorithm of the custom program was to first run RosettaDock, generating 3,000 high-resolution decoys. Each decoy was then parsed, checking whether each TbpB residue designated as important was within 10 Å of pTf, and deleting those decoys that failed on any residue. RosettaDock was then run again to generate as many new decoys as necessary to bring the total back up to 3,000, and the cycle repeated until all decoys met each of the designated distance constraints.

This program was used to generate models for both of the new structures *Ap*H87 and *As*H57 TbpB, as well as the previously solved structure from *Ap*H49 (16). For *Ap*H87, the residues deemed important were Tyr-95, Tyr-121, Tyr-174, and Arg-179, for *As*H57 the important residues were Phe-63 and Phe-152, and for *Ap*H49 they were Glu-112 and Phe-171. Initial perturbations were set to randomize both partners, move 3° and 8 Å, with a spin along the protein-protein axis. Monte Carlo minimization was used, and the decoys were generated in full-atom mode using multiple threads in parallel. For both the N-lobe and the full-length *Ap*H87 TbpB with pTF 1500 decoys were generated, running on 6 threads at once. The 10 decoys were chosen by their total score, which is determined by the scoring function.

Hydrogen/Deuterium Exchange (H/DX-MS) Experiments—Each H/DX-MS experiment consisted of two samples: free

TbpB (AsH57, *Ap*H49, or *Ap*H87) and the TbpB-pTf complex (*As*H57, *Ap*H49, or *Ap*H87). Each experiment was completed in quadruplicate, alternating between the receptors and complexes, therefore making future receptor cross-comparison possible. Ten microliters of TbpB was mixed with 5 μl HEPES buffer (10 mM HEPES, pH 7.0). Five microliters of heavy water (deuterated water, D_2O) was then added to this solution, mixed, and incubated immediately in a water bath at 20 °C, for 2 min. The labeled sample was then removed from the water bath, and 10 μl of cold quench solution (100 mM glycine hydrochloride, pH 2.3) was added. This sample was immediately injected onto a 10-μl loop, connected to an online immobilized pepsin reactor (2.5 cm by 200 μm internal diameter, assembled in-house) (Applied Biosystems, Concord, ON, Canada). An isocratic gradient of 3% ACN, 0.03% TFA, and 0.02% FA, at 4 μl/min was used to flow the intact labeled protein through the digestor column, and onto a C18 reversed-phase chromatography column (assembled in-house) (Applied Biosystems, Concord, ON, Canada). The peptides were separated with a step gradient of 5 to 90% ACN in 0.03% TFA and 0.02% FA over 14 min, and directly infused into a QSTAR Pulsar *i* quadrupole time-of-flight (QqTOF) mass spectrometer. All chromatography was carried out under ice, at 0–4 °C. Data were collected using Analyst QS^{TM} version 1.1 (Applied Biosystems).

To determine the TbpB peptides arising from the online pepsin digests, unlabeled peptides were prepared under the same conditions as mentioned above. Separated peptides were subjected to tandem mass spectrometry (MS/MS). The MS/MS spectral data were searched against the TbpB sequence (either *Ap*H49, *As*H57, or *Ap*H87), using an in-house licensed version of MASCOT 2.1, with conventional identification criteria ($\pm$0.5amu mass tolerance in MS and 0.8amu mass tolerance in MS/MS). The MASCOT search identified 58 usable peptides for AsH57 and peptides were then manually verified. Mass spectral data from each replicate H/DX-MS run was analyzed using Hydra software (25), using the method described by Ling *et al.* (26).

RESULTS

Phylogenetic Analysis—Through sequencing *tbpB* genes from our strain collection and combining them with sequences available from public databases, we compared TbpBs from *A. pleuropneumoniae* and *A. suis* to gauge the degree of sequence diversity (supplemental Fig. S1). Three TbpBs divergent from the one previously structurally characterized (16) were produced for structural studies and the structures of two of these TbpBs were obtained. Together with the published structure, these provide a reasonable representation of the sequence diversity (*red arrows*, supplemental Fig. S1). A sequence alignment between the three TbpBs for which structural information is available is shown in Fig. 1. The results illustrate that there is significant sequence variation in the handle (*blue color*) and barrel (*green color*) domains of the N-lobe of TbpB (Fig. 1, *upper panel*) that primarily resides in loops on cap area of the N-lobe (*lower panel*).

Overall Structural Features—The structures of TbpBs from *A. suis* strain H57 (*As*H57) and *A. pleuropneumoniae* strain H87 (*Ap*H87) (Table 1) have a similar fold to the previously

characterized TbpB from *A. pleuropneumonae strain* H49 (*Ap*H49), which consists of two globular domains, the N and C lobes (N-lobe: AsH57 TbpB residues 27–342, *Ap*H87 TbpB residues 26–294; C-lobe: *As*H57 TbpB residues 343–577, *Ap*H87 TbpB residues 295–528). Each lobe is comprised of a β-barrel element flanked by an adjacent handle domain (Fig. 1 and supplemental Fig. S2). The β-barrel configuration of N- and C-lobes consist of an eight-stranded β-barrel with, in case of *As*H57 TbpB, two additional surface-exposed anti-parallel β-strands in the large N-lobe loop region between the β-strand L8β1 and β8 (Fig. 1). In both *As*H57 and *Ap*H87 TbpBs, the handle domain from N-lobe (*As*H57 TbpB: residues 49–172; *Ap*H87 TbpB: residues 49–141) consists of a four stranded anti-parallel β-sheet supported by an short α-helix, which packs together with the adjacent β-barrel forming a globular core, N-lobe, that is linked to the C-lobe handle domain (Fig. 1).

The C-lobe handle domains (*As*H57 TbpB residues 343–431, *Ap*H87 TbpB residues 295–382), as in *Ap*H49 TbpB, are composed of six-stranded anti-parallel β-sheets stacked between the C-lobe β-barrel core (*As*H57 TbpB residues 432–577, *Ap*H87 TbpB residues 383–528) and two surface-exposed anti-parallel β-strands (Fig. 1). The N- and C-lobe of both TbpB structures form two independent structural domains that are maintained in an orthogonal orientation by an evolutionary conserved hydrophobic core flanked by two salt bridges.

The N-terminal Anchoring Peptides Have Different Conformations—The conformation of the N-terminal anchor peptide (the residues preceding the leucine 50 residue of the first β-strand) of the *Ap*H57 TbpB differs from the two other TbpBs. The *Ap*H87 TbpB N terminus rotates 118 degrees at Lys-43 and extends into a long α-helix stacked on the N-lobe (Fig. 2). In the crystal, the N-terminal peptide of *Ap*H49 and *As*H87 TbpB (respectively residues 1–41, and 1–43) is oriented toward the C-lobe, interacting the C terminus by intra-chain contact. Crystallized in a different space group C222$_1$, the *Ap*H57 TbpB N terminus (residues 1–43) extends along the N-lobe and also interacts the C-lobe terminal residues but from the adjacent monomer in the unit cell. These two alternative conformations support the argument that TbpB uses its N-terminal region as a flexible anchoring peptide to extend above the capsular layer to bind Tf from the extracellular millieu and recruit it toward the outer membrane surface.

N-lobe of TbpB Varies in Sequence and Structure between Porcine Pathogens—The "cap" area is composed of the loops protruding from the N-lobe β-barrel and handle domain (loop 1, 3, 5, 8, 10, 12 in addition to the long insertion within the loop 4 that points toward the Cap area in *Ap*H57 TbpB) (Fig. 1 and supplemental Fig. S2). This cap region represents the most variable region between the three known TbpB structures, and between all TbpBs in general. Structural alignments of N-lobe domain of *As*H57 and *Ap*H87 TbpBs yield an RMSD of 1.7 Å between these two domains, and 3.4 Å and 0.78 Å when respectively compared with *Ap*H49 TbpB.

Focusing on the putative Tf-binding site previously proposed on the cap area (16), a comparison of the cap surfaces reveals many differences between *As*H57 TbpB and the two other TbpB receptors. Long insertions in the outward facing loop region within the N-lobe β-barrel and handle domain of *As*H57

A. *ApH49 TbpB*

B. *ApH87 TbpB*
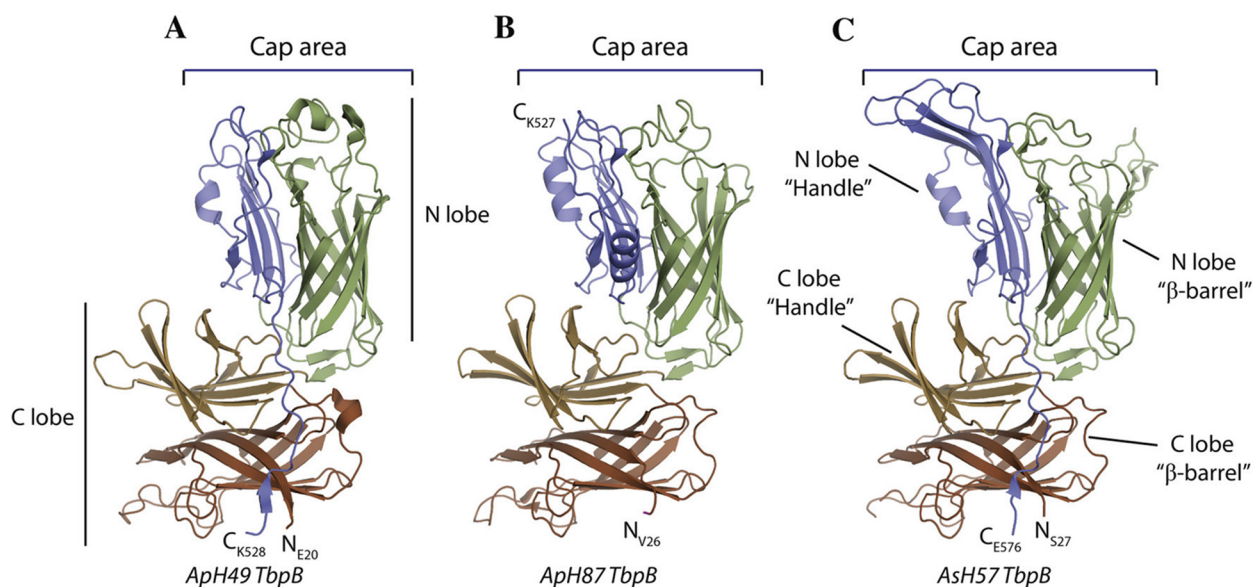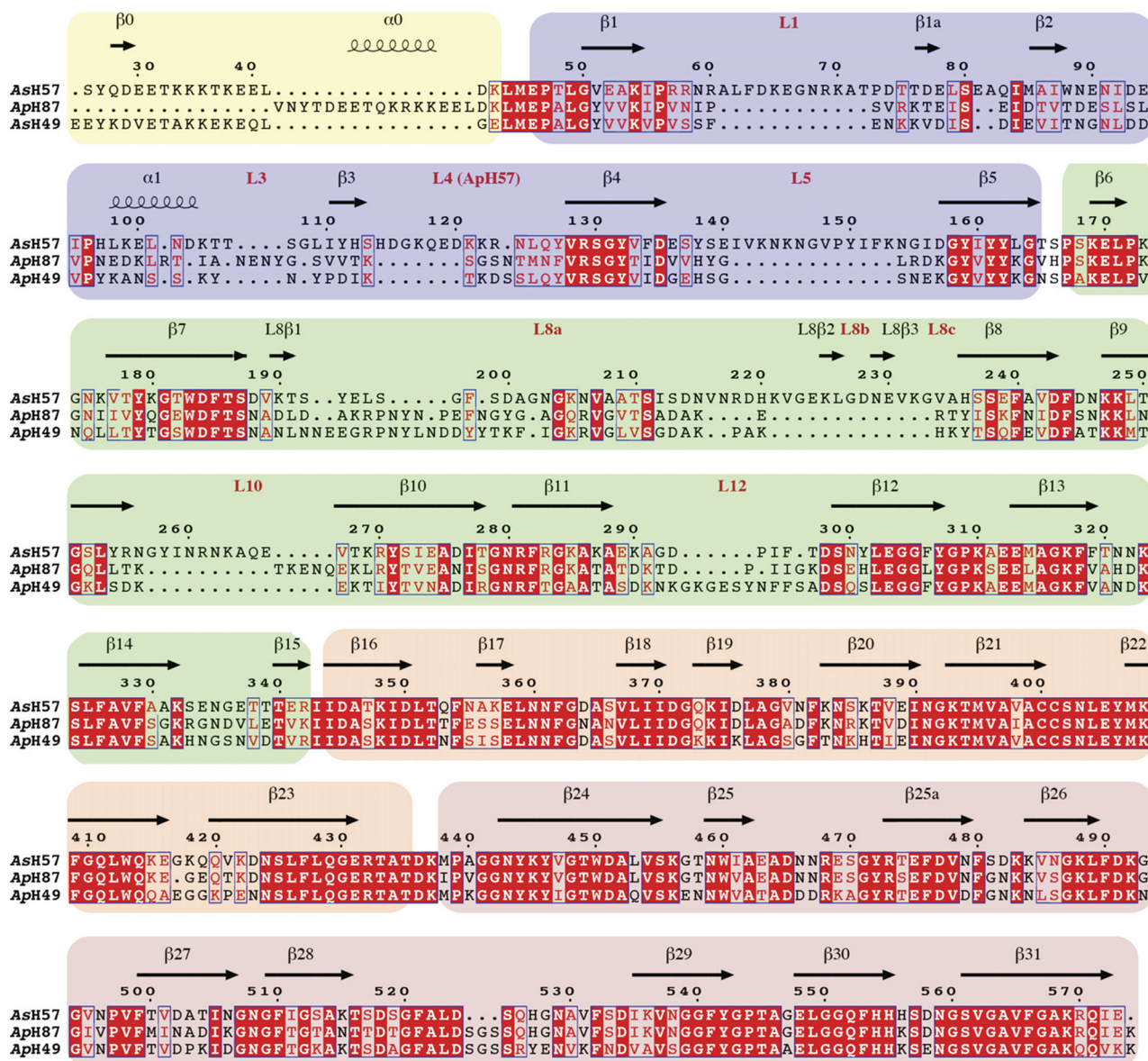
C. *AsH57 TbpB*

TABLE 1

Data collection and refinement statistics for *As*H57 and *Ap*H87 TbpB

	*As*H57 TbpB[27–577]	*Ap*H87 TbpB[26–528]
Data collection		
Space group	P2$_1$	C222$_1$
Cell dimensions		
a, b, c (Å)	90.7, 74.5, 106.4	132.6, 151.3, 90.3
a, b, g (°)	90.0, 105.7, 90.0	90, 90, 90
Resolution (Å)	50-2.1 (2.17-2.1)[a]	50-2.1 (2.17-2.1)
R_{sym} or R_{merge}	0.145 (0.50)	0.093 (0.45)
$I/\sigma I$	15.7 (3.1)	28.6 (4.4)
Completeness (%)	99.7 (99.2)	99.9 (99.8)
Redundancy	3.9 (2.3)	13.7 (10.1)
Refinement		
Resolution (Å)	44.76-2.1	47.14-2.1
No. reflections	75629	50535
R_{work}/R_{free}	0.17/0.21	0.16/0.20
No. atoms	9509	4595
Protein	8589	4033
Glycerol	30	90
Cacodylic acid	0	5
Water	890	498
B-factors	50.1	64.5
Protein	50.5	62.8
Ligand/ion	69.6	98.6
Water	44.8	71.3
R.m.s. deviations		
Bond lengths (Å)	0.007	0.006
Bond angles (°)	1.071	1.062

[a] Highest resolution shell is shown in parenthesis.
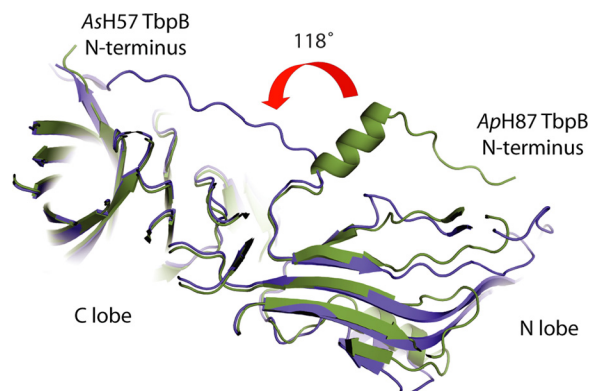
FIGURE 2. **The flexible N terminus-anchoring region of TbpB.** Clipped schematic representation of superimposed *As*H57 TbpB (colored in *blue*) and *Ap*H87 TbpB (colored in *green*). The N- and C-lobe are indicated, and the N terminus of both TbpBs is labeled. The *red curved arrow* illustrates the 118° rotation between N-terminal extremities of *As*H57 and *Ap*H87 TbpBs. This angle is defined by the position of Thr-33 with respect to Lys-43 in the *Ap*H87 and *As*H57 TbpBs.

TbpB results in a larger surface exposed area that is 69 Å in length compared with that of *Ap*H49 or *Ap*H87 TbpB, whose cap areas extend 38 and 44 Å, respectively (Fig. 3*A*).

*Ap*H49 TbpB-pTf Sites of Interaction—Based on our previous model of the Tf-*Ap*H49 TbpB recognition, we mapped the key binding elements involved in the pTf-binding site onto the two new TbpB structures. The first common characteristic shared between the three putative binding pockets is the large positive surface spread on the cap region, which was previously pro-

posed to interact with the Tf C-lobe. This positively charged interface involved loops from both the β-barrel and the handle domain but, in the case of *As*H57 TbpB, the site is exclusively localized on its large loop and β-strand (β4 and β5) insertions extended from the handle domain (Fig. 3*B*).

Characterization of *Ap*H49 TbpB demonstrated Phe-171 as a crucial residue for Tf-binding function. Based on structure overlapping, we detected an equivalent aromatic residue, Tyr-174 in *Ap*H87 at the similar position to *Ap*H49 TbpB Phe171 (Fig. 3*B*), which is not apparent from sequence alignments (Fig. 1, *upper panel*). The cap region of *As*H57 TbpB is more divergent than the two other crystallized TbpBs and there were no obvious residues in the binding interface that corresponded to Phe-171 or other critical residues from *Ap*H49 TbpB. These variations are essentially due to major structural differences in loop organization of the cap region (Fig. 3*B*).

Although the cap interface of *As*H57 TbpB does not appear to be conserved with *Ap*H49 and *Ap*H87, it still has a conserved feature of two surface exposed hydrophobic residues (Phe-63 and Phe-152) located within the positively charged cap area (Fig. 3*B*). However, these phenylalanines are localized on the handle domain loop instead of β-barrel as in the *Ap*H87 and *Ap*H49 TbpB structures.

Surface Plasmon Resonance Reveals the Binding Affinities of TbpBs with pTf—Surface plasmon resonance was used to quantify binding affinity between different TbpB preparations and covalently immobilized pTf on a BiacoreX (Table 2 and the supplemental Fig. S3). *Ap*H49 and *Ap*H87 TbpB share closely related cap areas, and an equally similar pTf affinity of 44 and 60 nM, respectively. The *As*H57 TbpB has a lower binding affinity of 120 nM. Our SPR data are in agreement with a previous characterization of *Ap*H49 TbpB by isothermal titration calorimetry that revealed a dissociation constant of 55 nM (16).

SPR data from the TbpB receptors did not match to a 1:1 Langmuir binding model. Difficulty in fitting our kinetic data to a 1:1 model could be a consequence of ligand/analyte heterogeneity, or two-step binding kinetics. To discriminate between these models we monitored the effect of several saturation times on the dissociation events of TbpBs (supplemental Fig. S3 and Table S1): in case of heterogeneous analyte or two-step binding kinetics, the dissociation will slow as the duration of the injection is increased. Comparing the dissociation phase that occurs after variation in the saturation time, we show that the dissociation curves are not affected by the contact time (supplemental Fig. S3) and that the "heterogeneous ligand" binding model best fits the data.

Mutational Analysis of AsH57 and ApH87 TbpB—The pTf-binding site determined for the previously characterized *Ap*H49 TbpB has common features with the two homologous TbpB structures presented herein. They all share the feature of a positively charged region in the N-lobe cap sur-

FIGURE 1. **Structural alignment of three TbpBs from the swine pathogenic strains *Ap*H49, *As*H57, and *Ap*H87.** Background colors *yellow*, *blue*, *green*, *orange*, and *peach* denote the domain architecture of the N-terminal anchoring peptide, then the handle and β-barrel domain from the N- and C-lobe, respectively. The secondary structure elements and loops from the cap area are shown above the sequences according to the TbpB labeling nomenclature is described in the supplementary Fig. S1. Identical residues and conserved residues are *highlighted* and boxed *red*. *A, B,* and *C*, respectively are cartoon representations of *Ap*H49 TbpB from residues 24–528 (PDB code: 3HOL Moraes *et al.*, 16) (*A*), *Ap*H87 TbpB from residues 26–528 (PDB code: 3PQS determined in this study) (*B*), and *As*H57 TbpB from residues 27–577 (PDB code: 3PQU determined in this study). The N-lobe β-barrel and handle domain are, respectively, colored in *green* and *blue*; the C-lobe β-barrel and handle domain are, respectively, colored in *brown* and *sand*. The cap area is labeled.
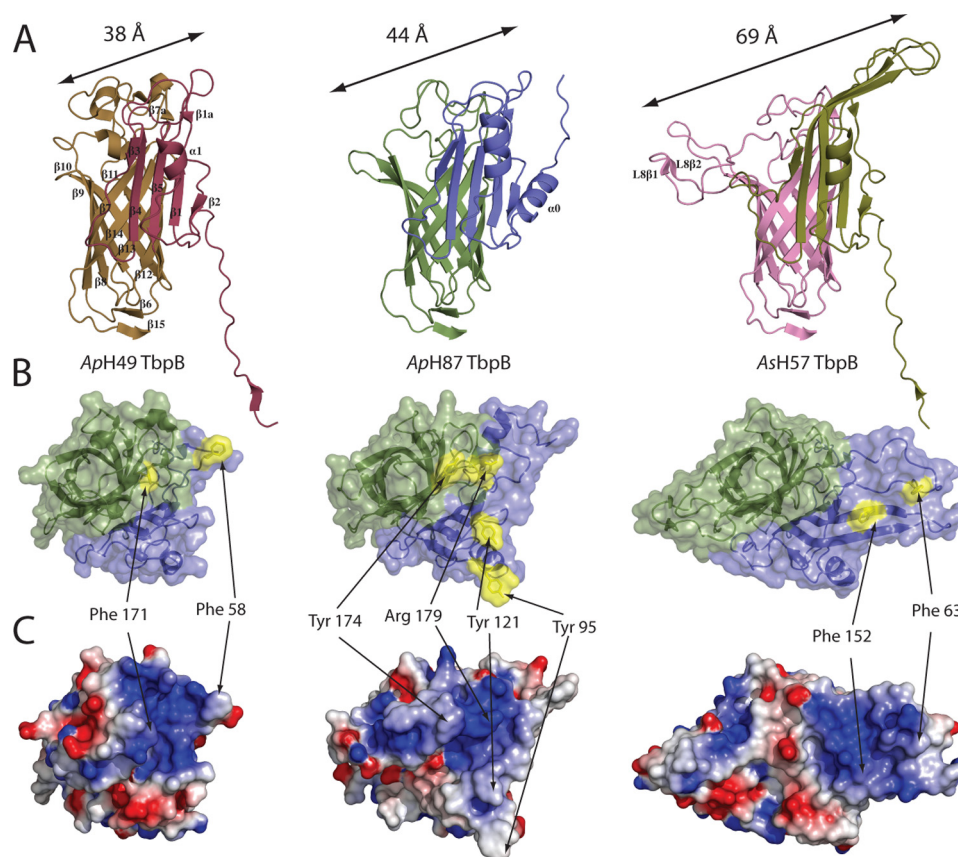
FIGURE 3. **A comparison of TbpB N-lobes.** *A*, cartoon representation of TbpB N-lobe from *Ap*H49, *Ap*H87, and *As*H57 TbpBs. The common secondary structure elements are labeled on *Ap*H49 TbpB, and additional secondary structural elements found in *Ap*H87 or *As*H57 are labeled. *B*, Cap Tf-binding region of the TbpB N-lobe. Structures are all in the same orientation with a focus on the "cap" region and loops of N-lobe viewed from the *top*. The β-barrel domain and handle domain are, respectively, colored in *green* and *blue*. The aromatic surface exposed amino acids from the cap area are highlighted in *yellow* and labeled. *C*, cartoon and electrostatic surfaces are shown for each of *Ap*H49, *Ap*H87, and *As*H57 TbpBs with *blue* and *red* denoting positive and negative potential.

TABLE 2

Rate and affinity constants for binding of *Ap*H49, *As*H57, and *Ap*H87 TbpB wild types and mutants to pTf

The rate and affinity constants were determined from sensorgrams recorded for the binding of wild type and mutant TbpBs to pTf according to the "heterogeneous ligand" binding model.

Protein	k_{on1}	k_{off1}	K_d
	$M^{-1} s^{-1}$	s^{-1}	
*Ap*H49 TbpB	1.75×10^5	7.7×10^{-3}	44 ± 1 nM
*Ap*H87 TbpB	2.12×10^5	1.28×10^{-2}	60 ± 2 nM
*Ap*H87 TbpB Y121A	1.50×10^5	3.06×10^{-2}	203 ± 8 nM
*Ap*H87 TbpB Y95A	2.94×10^4	1.17×10^{-2}	585 ± 11 nM
*Ap*H87 TbpB Y174A	2.61×10^2	2.33×10^{-3}	8.9 ± 0.4 μM
*Ap*H87 TbpB R179E	nd[a]	nd[a]	6.1 ± 0.6 μM
*As*H57 TbpB	2.52×10^5	3.06×10^{-2}	120 ± 4 nM
*As*H57 TbpB F152A	6.10×10^4	2.43×10^{-2}	405 ± 8 nM
*As*H57 TbpB F63A	3.29×10^5	1.07×10^{-1}	326 ± 11 nM

[a] nd, not determined.

face and all contain surface exposed aromatic residues within this region. In *Ap*H49 TbpB this surface exposed aromatic was shown to be essential for binding pTf. Thus all exposed aromatic amino acids from the putative binding sites of *As*H57 and *Ap*H87 TbpBs were mutated to alanine and the resulting mutant proteins tested for binding by SPR. Table 2 displays the affinity constants from the wild type and mutant TbpBs. The SPR experiments indicate that Tyr-174, Tyr-121, and Tyr-95 from *Ap*H87 TbpB are involved in pTf recognition, with respective pTf affinities of 8.9 μM, 203 nM, and 585 nM compared with 60 nM for the wild type *Ap*H87

TbpB. Tyr-174 from *Ap*H87 has the strongest impact on the pTf interaction and is localized near to the essential Phe-171 from *Ap*H49 TbpB (Fig. 4*B*) (16). In the case of *As*H57 TbpB, direct binding experiments identify two phenylalanines involved in pTf recognition; Phe-63 and Phe-152 are located in the large protruding loop L1 and the extended β5 strand from the N-lobe handle domain with their side-chains solvent exposed (Fig. 4*C*).

The loops protruding from the N-lobe β-barrel were also proposed to mediate electrostatic interactions between pTf and TbpB (16). To probe the role of the electropositive surface of the TbpB N-lobe Cap region on pTf affinity, we mutated the conserved, solvent-exposed Arg-179 to Glu within *As*H87 TbpB, (equivalent to Arg-175 in *Ap*H49 TbpB). The resultant mutant protein was purified and examined using direct binding assays by SPR. The pTf-binding experiments indicate a drastic lost in binding efficiency of the R179E mutant compared with wild type (60 nM to 6.1 μM binding affinities) (Table 2). The substitution of a single positively charged residue in the cap area to glutamic acid is sufficient to abrogate the pTf binding activity of the *Ap*H87 TbpB.

Models of TbpB AsH57 and ApH87 Bound to pTf—Rosetta docking was performed using the C-lobe of pTf (iron loaded) and the structures of the N-lobes of *Ap*H87 or *As*H57 TbpBs. In these docking experiments the mutational data were used to add constraints to the docking algorithm. For both TbpBs, the
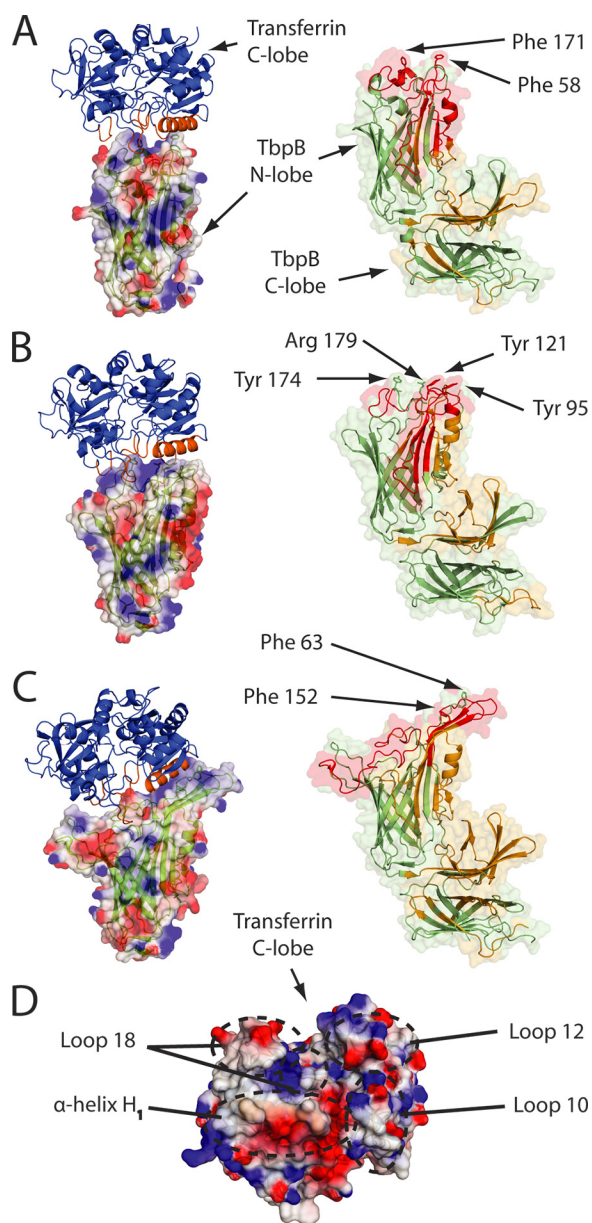
FIGURE 4. **Rosetta-docked models of TbpBs bound to pTf, supported by H/DX-MS.** *A–C*, representation of H/DX-MS experiments (*right panel*) and Rosetta-docked models (*left panel*) of *Ap*H49 TbpB (*A*), *Ap*H87 TbpB (*B*), and *As*H57 TbpB (*C*) bound to pTf. On the *right* is the schematic representation of the TbpBs: colored in *red* are the regions protected in presence of transferrin, in *orange* are indicated the unprotected sequence, and in *light green* are regions where there is no information by mass spectrometry (sequence coverage that are missing). At the *left* are shown the docking models with TbpB electrostatic potential surface and carton-illustrated pTf C-lobe. The pTf C-lobe is colored in *blue* and binding interface with TbpBs is in *orange*. All TbpB structures from H/DX-MS and Rosetta-docked models are shown in the same orientation. *D*, TbpB binding area on pTf is proposed on *Ap*H49, *Ap*H87, and *As*H57 TbpB the Rosetta-docked models. A top view of the electrostatic potential surface of the putative TbpB-binding site on pTf is illustrated with structural elements in the binding site (α-helix H_1 and the loop elements L_{15}, L_{18}, and L_{23}) labeled.

top 1% of the highest scoring docked models were examined manually, and one heavily favored orientation was found for each (supplemental Fig. S4). These predominant models were homologous within 20 of the top 30 decoys for their respective docking runs. The second most favored orientation had only 3 and 4 homologues each. Though *Ap*H87 and *As*H57 TbpB have

many major differing structural features, especially around the proposed pTf binding site, the predicted docking orientations of both structures were nearly identical (Fig. 5). Because of this similarity, a new docked model was generated for the previously reported *Ap*H49 TbpB structure, incorporating important residue data as constraints (described under "Experimental Procedures"). The majority of the models (17 of the top 30) resulted in a nearly identical orientation to those of *As*H57 and *Ap*H87 models.

In our three independently generated models, the TbpB-binding interface on pTf is conserved. The C1 and C2 domains of the transferrin C-lobe bind to the handle and β-barrel domain of TbpBs, respectively (Fig. 5). Porcine transferrin docks on TbpB with the α-helix H_1 (residues 352–366) and the loop elements L_{15} (residues 507–513 and 519–521), L_{18} (residues 555–559), and L_{23} (residues 624–627 and 633–636). A conserved binding pattern emerges from the Rosetta docked models, which suggests the helix and loop elements H_1, L_{15}, L_{18}, and L_{23} of pTf form the TbpB binding interface on pTf (Fig. 5). The negatively charged α-helix H_1 and loop23 (consisting of the motif CSSS, residues 624–627) of pTf binds the positively charged cap area of the TbpBs. Loop15 of pTf makes several contacts with TbpBs, but one key residue contact that is central to each model is the positively charged Arg-509, which is oriented toward a negative pocket in the canyon formed between the N-lobe β-barrel and handle domains.[4] Loop18 (non uniformly charged) of pTf makes contact on the β-barrel domain but we note that the electrochemical environment on TbpB is not maintained between the three-studied TbpBs.

Porcine Transferrin Binds TbpB on the Cap Area—To localize and confirm the Tf-binding site location, we performed H/DX-MS. Results from experiments with TbpB from three strains; *A. pleuropneumoniae* H49 and H87, and *A. suis* H57 alone, and upon complex formation with pTf, are presented in Fig. 5. For the *Ap*H49, *As*H57, and *Ap*H87 TbpBs, a total of 57, 58, and 54 pepsin-digested peptides, respectively, could be utilized, covering 46, 45, and 43% of the protein sequences and 69, 60, 61% of the respective cap region (supplemental Fig. S5). The isotopic mass shift due to deuterium incorporation in TbpB fragments were detected using a QStar pulsar mass spectrometer, and analyzed via Hydra software, as described under "Experimental Procedures." Despite incomplete sequence coverage of the receptors with a pepsin digestion, the protected sequences of the three-studied TbpBs are all located on the N-lobe domain and more precisely localized along the cap area of each of the porcine TbpBs studied (Fig. 4).

DISCUSSION

Structural Features of TbpBs—The two new structures reported in this study demonstrate that the overall structural features of TbpBs are conserved despite considerable sequence variation and size differences. Each lobe is comprised of an 8-stranded β-barrel with a 5-stranded handle domain in the N-lobe and a 6-stranded handle domain in the C-lobe (supplemental Fig. S2). The size and sequence differences are largely
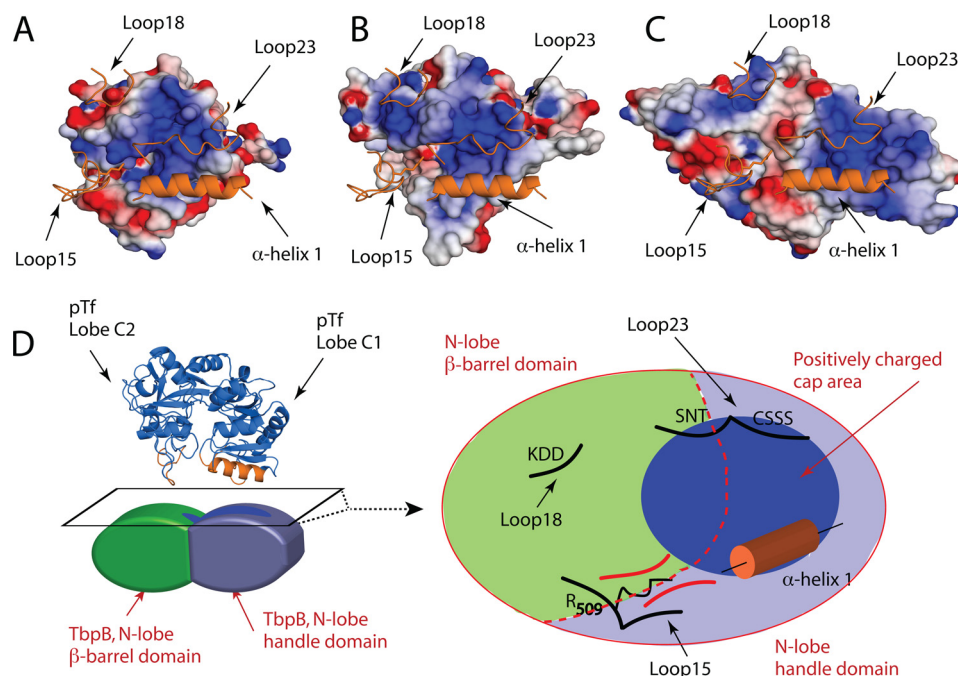

FIGURE 5. **The conserved elements of the TbpB-pTf Binding Interface.** *A–C*, N-lobe Cap areas of *Ap*H49, *Ap*H87, and the *As*H57 TbpBs are represented in *A*, *B*, and *C*, respectively. An *orange* cartoon representation is the pTf predicted TbpB-binding elements from the Rosetta-docked TbpB-pTf models. In each model, the arginine 509 from the loop 15 of pTf is shown in *stick representation*. *D*, *top surface* of the TbpB N-lobe demarking the barrel and handle domain in *red-dotted line*. The negatively charged cap area is represented in *dark blue*, the β-barrel in *green*, and the handle domain in *blue*. Structural elements from the pTf C-lobe localized at the interface with TbpBs are drawn in *black* (loop 15, 18, 23, and α-helix1). The loop 23 and the helix H1 (*orange*) dock on the TbpB positively charged cap area, driven by electrostatic interaction. pTf loop 15 makes contact with TbpB at the between the β-barrel and handle domain, where the Arg-509 seats deeply in the canyon formed by the two domains of the N-lobe.

manifested by variation in the loops that constitute the Cap region of the N-lobe. There is a conserved interaction between the N-terminal lobe that contains the Tf binding interface and the relatively conserved C-lobe, in an orthogonal orientation. Although the C-lobe is not directly involved in Tf binding, its presence and conserved interaction with the N-lobe could be important for the receptor function *in vivo*. The lack of sequence variation in the C-lobe compared with the N-lobe may infer a conserved interaction with other surface components.

In the *Ap*H49 and *As*H57 proteins the extended N-terminal anchoring peptide interacts through hydrogen bonds with the C-lobe. In the *Ap*H87 structure the anchoring peptide assumes a different conformation that appears to be stabilized by interchain contacts with the adjacent TbpB in the crystal lattice. The complete N-terminal anchoring peptides consist of more than 43 residues that could equate to ~100 Å in length if in an extended conformation in solution. Thus the two observed conformations (Fig. 2) suggest that the N-terminal membrane-anchored peptide may allow the TbpB receptor to adopt an extended orientation to more effectively capture host Tf in the presence of the polysaccharide capsular layer.

TbpB Conservation of the pTf-binding Sites—Based on our pTf-TbpB model, there are substantial variations in the TbpB N-lobe Cap regions, however all strains studied permit high affinity specific binding interactions with Tf. The cap region involved in pTf recognition is directly exposed to the host environment, including the immune defense elements. The sequence and structural variation of this cap region likely is a mechanism for immune evasion, providing decoy epitopes that

vary between strains so that a primarily strain-specific immune response is induced (27). Because the different receptor proteins need to retain the ability to bind to transferrin in a similar fashion, there should be conserved features that could otherwise induce a cross-reactive immune response. Thus there would be selective pressure for directing the immune response to variable regions or to accomplish a somewhat conserved Tf interaction by variable means.

Based on the three solved structures of TbpB we can classify the pTf-binding sites into at least two groups: *Ap*H49 and *Ap*H87 TbpBs that share similarities in the loop's cap area, and *As*H57 TbpB that has a large extended loop containing some new secondary structural elements. The results from this study suggest that *As*H57 TbpB adopts a novel interaction pattern with pTf, as the binding interface appears highly modified compared with *Ap*H87 and *Ap*H49 (Fig. 3*A*). The cap area of *As*H57 TbpB is also identified by H/DX-MS experiments as an interfacial region with pTf. The two protruding loop regions of *As*H57 TbpB create a larger surface area buried in the model (~4400 Å^2) with pTf (Fig. 4*C*). The strikingly different loop structure while maintaining interactions with the same regions of pTf has important implications on how this diversity is created and on potential barriers to horizontal exchange of antigenic diversity.

Using a structure-based approach, TbpB mutants were selectively designed to probe related effects on function with the goal to more precisely define the binding activity of these prokaryote pTf receptors. Based on previous studies of *Ap*H49 TbpB (16), we first focused on the solvent exposed aromatic residues accessible from the cap area of *As*H57 and *Ap*H87 TbpBs. SPR binding experiments with all the alanine substitutions of phe-

nylalanine and tyrosine residues within the putative binding sites, revealed that similar amino acids to the *Ap*H49 TbpB Phe-171 are also required for the pTf binding of *As*H57 and *Ap*H87 TbpBs. These binding experiments point to the importance of the Tyr-95 and Tyr-121 and the structurally conserved Tyr-174 on *Ap*H87 TbpB (Fig. 4*B*), and the non-conserved Phe-63 and Phe-152 on *As*H57 TbpB (Figs. 4*C*). Interestingly, the phenylalanines 63 and 152 are localized on the protruding loop L1 and the extended β5-strand from the handle domain instead of the β-barrel as in the case of the essential aromatic residues from *Ap*H49 and *Ap*H87 TbpBs (Fig. 4).

Despite the loop variation between the pTf-binding sites, the swine pathogen TbpBs share similar characteristics for capturing porcine Tf. In addition to the essential Phe and Tyr hydrophobic residues on the cap area, the pTf-TbpB recognition seems to depend on a positively charged interface, which is predicted at the pTf interface by computational Rosetta docking and by experimental HDX-MS data. Indeed the putative pTf-binding sites from the three TbpB structures all maintain a positively charged interface on the cap area, which matches to the neighborhood of the essential Phe and Tyr (Fig. 3*B*). To test the pTf binding dependence toward this positively charged area, we prepared an *Ap*H87 TbpB mutant in which the Arg-179 has been substituted by a glutamic acid. This mutant allowed us to measure the deficiency in pTf-binding caused by a partial charge disruption in the putative binding site. The mutation was sufficient to disrupt the pTf binding function by insertion of a single negatively charged amino acid.

All three TbpB structures present similar characteristics involving aromatic and positively charged residues, but they show variability in localization. The binding contributors from both *Ap*H49 TbpB and *Ap*H87 have partial similarity in arrangement (Fig. 3*B*), but differ more drastically with the structurally non-conserved *As*H57 TbpB binding site (Fig. 3*B*). The independent Rosetta docked models from *Ap*H49, *Ap*H87, and *As*H57 predict the N-lobe Cap area as the pTf-binding pocket of the swine-related TbpBs. The H/DX-MS experimental data validates our three Rosetta docked models, confirming the Cap area as the TbpB/pTf interface. Although H/DX-MS overall TbpB sequence coverage of the three TbpB strains was low, coverage of the cap regions was quite high, with most of the missing coverage being attributed to the rigid β-barrels in each of the TbpB lobes. In agreement with our models, most of the protruding loops from the cap area are protected in presence of pTf (Fig. 4).

Despite the divergence in the TbpB interface, the conserved physicochemical properties of the binding sites support idea that these TbpB could target a common binding-site on pTf. Based on our Rosetta docking experiments, TbpB receptors bind to the same surface on pTf (Figs. 4 and 5). Our three independently generated TbpB/pTf binding models suggest the loop elements L15, L18, L23, and the α-helix H1 as the TbpB-binding site on pTf.

Despite a high sequence homology between Tfs from different species (70% between pTf and hTf C-lobes), the TbpB binding function for Tf is host specific. Interestingly, amino-acids from pTf that are predicted to contact the porcine pathogen TbpBs are not conserved when compared with hTf (supplemental Fig. S6), sug-gesting that pathogens have adapted to discriminate specific host Tf with higher affinity; or a host evolution as defense mechanism to avoid infection from Tf-based pathogens.

Implication in Vaccine Design—TbpBs have been targeted for development of vaccines for a number of human and veterinary pathogens due to the critical role they mediate and their resulting invariant presence in clinical disease isolates (14, 27–29). Although they are capable of inducing a protective immune response, there is an insufficient cross-protective response induced by individual intact receptor proteins to be considered as suitable vaccine antigens. The fact that these proteins mediate a conserved interaction with the host Tf provided some optimism of ultimately targeting conserved regions of the proteins for developing a more cross-protective antigen. Furthermore, if common Tf-binding regions could be targeted by the immune response, the bacteria would be unable to evade the immune response by ongoing antigenic variation as this could also compromise the critical function mediated by TbpB.

The results from this study demonstrate that there is no obvious conserved Tf-binding region in the N-terminal lobe common to all the TbpBs from porcine pathogens that could simply be used as vaccine antigen capable of inducing a cross-protective immune response. It seems evident that the divergent TbpBs accomplish binding of porcine Tf with common, but not identical, features and that further study will be needed to fully appreciate the molecular details of this interaction. Clearly the most informative approach would be determining structures of pTf-TbpB complexes but these have been evasive to date, and a combination of alternate approaches may need to be considered. A detailed appreciation of the pTf-TbpB interaction may ultimately provide insights on how to develop one or more receptor derivatives or mimics capable of inducing a cross-protective response against all porcine pathogens. Expanding this approach to developing vaccines against human pathogens will require gathering structural information on a large set of TbpB homologues to develop broad-spectrum protection again multiple pathogenic species.

REFERENCES

1. Ratledge, C., and Dover, L. G. (2000) *Annu. Rev. Microbiol.* **54,** 881–941
2. Gray-Owen, S. D., and Schryvers, A. B. (1996) *Trends Microbiol.* **4,** 185–191
3. Cornelissen, C. N., Kelley, M., Hobbs, M. M., Anderson, J. E., Cannon, J. G., Cohen, M. S., and Sparling, P. F. (1998) *Mol. Microbiol.* **27,** 611–616
4. Yu, R. H., and Schryvers, A. B. (1993) *Microb. Pathog.* **15,** 433–445
5. Cornelissen, C. N., Biswas, G. D., Tsai, J., Paruchuri, D. K., Thompson, S. A., and Sparling, P. F. (1992) *J. Bacteriol.* **174,** 5788–5797
6. Retzer, M. D., Yu, R., Zhang, Y., Gonzalez, G. C., and Schryvers, A. B. (1998) *Microb. Pathog.* **25,** 175–180
7. Zak, O., and Aisen, P. (1986) *Blood* **68,** 157–161
8. Baltes, N., Hennig-Pauka, I., and Gerlach, G. F. (2002) *FEMS Microbiol. Lett.* **209,** 283–287
9. Schryvers, A. B., and Gonzalez, G. C. (1990) *Can J. Microbiol.* **36,** 145–147
10. Cheng, Y., Zak, O., Aisen, P., Harrison, S. C., and Walz, T. (2004) *Cell* **116,** 565–576

11. Kaplan, J. (2002) *Cell* **111,** 603–606
12. Pizza, M., Scarlato, V., Masignani, V., Giuliani, M. M., Aricò, B., Comanducci, M., Jennings, G. T., Baldi, L., Bartolini, E., Capecchi, B., Galeotti, C. L., Luzzi, E., Manetti, R., Marchetti, E., Mora, M., Nuti, S., Ratti, G., Santini, L., Savino, S., Scarselli, M., Storni, E., Zuo, P., Broeker, M., Hundt, E., Knapp, B., Blair, E., Mason, T., Tettelin, H., Hood, D. W., Jeffries, A. C., Saunders, N. J., Granoff, D. M., Venter, J. C., Moxon, E. R., Grandi, G., and Rappuoli, R. (2000) *Science* **287,** 1816–1820
13. Lissolo, L., Maitre-Wilmotte, G., Dumas, P., Mignon, M., Danve, B., and Quentin-Millet, M. J. (1995) *Infect. Immun.* **63,** 884–890
14. Danve, B., Lissolo, L., Mignon, M., Dumas, P., Colombani, S., Schryvers, A. B., and Quentin-Millet, M. J. (1993) *Vaccine* **11,** 1214–1220
15. Gray-Owen, S. D., and Schryvers, A. B. (1993) *Microb Pathog* **14,** 389–398
16. Moraes, T. F., Yu, R. H., Strynadka, N. C., and Schryvers, A. B. (2009) *Mol. Cell* **35,** 523–533
17. del Río, M. L., Gutiérrez-Martin, C. B., Rodríguez-Barbosa, J. I., Navas, J., and Rodríguez-Ferri, E. F. (2005) *FEMS Immunol. Med. Microbiol.* **45,** 75–86
18. Bahrami, F., Ekins, A., and Niven, D. F. (2003) *Vet. Microbiol.* **94,** 79–92
19. Gonzalez, G. C., Caamano, D. L., and Schryvers, A. B. (1990) *Mol. Microbiol.* **4,** 1173–1179
20. Kabsch, W. (1993) *J. Appl. Crystallogr.* **26,** 795–800
21. McCoy, A. J., Grosse-Kunstleve, R. W., Adams, P. D., Winn, M. D., Storoni, L. C., and Read, R. J. (2007) *J. Appl. Crystallogr.* **40,** 658–674
22. Emsley, P., and Cowtan, K. (2004) *Acta Crystallogr. D Biol. Crystallogr.* **60,** 2126–2132
23. Murshudov, G. N., Vagin, A. A., and Dodson, E. J. (1997) *Acta Crystallogr D Biol. Crystallogr.* **53,** 240–255
24. Gray, J. J., Moughon, S., Wang, C., Schueler-Furman, O., Kuhlman, B., Rohl, C. A., and Baker, D. (2003) *J. Mol. Biol.* **331,** 281–299
25. Slysz, G. W., Baker, C. A., Bozsa, B. M., Dang, A., Percy, A. J., Bennett, M., and Schriemer, D. C. (2009) *BMC Bioinformatics* **10,** 162
26. Ling, J. M., Shima, C. H., Schriemer, D. C., and Schryvers, A. B. (2010) *Mol. Microbiol.* **77,** 1301–1314
27. Rossi-Campos, A., Anderson, C., Gerlach, G. F., Klashinsky, S., Potter, A. A., and Willson, P. J. (1992) *Vaccine* **10,** 512–518
28. Myers, L. E., Yang, Y. P., Du, R. P., Wang, Q., Harkness, R. E., Schryvers, A. B., Klein, M. H., and Loosmore, S. M. (1998) *Infect. Immun.* **66,** 4183–4192
29. Potter, A. A., Schryvers, A. B., Ogunnariwo, J. A., Hutchins, W. A., Lo, R. Y., and Watts, T. (1999) *Microb. Pathog.* **27,** 197–206